Elastic Resonance Scattering Study of Protons on Aluminium

By

Muhammad Ali

Department of Physics
Quaid-i-Azam University
Islamabad, Pakistan

January, 2013.

This work is submitted as a dissertation in partial fulfillment of the requirement for the degree of

MASTER OF PHILOSOPHY IN PHYSICS

Department of Physics
Quaid-i-Azam University
Islamabad, Pakistan

Certificate

It is certified that the work contained in this dissertation is carried out and completed by Mr. Muhammad Ali under my supervision at the Experimental Physics Directorate (EPD) Laboratory, National Centre for Physics (NCP), Islamabad, Pakistan.

Supervisor:

Dr. Sajjad Hussain Bhatti
Assistant Professor,
Department of Physics,
Quaid-i-Azam University,
Islamabad, Pakistan.

Submitted through:

Prof. Dr. Muhammad Zakaullah
Chairman,
Department of Physics,
Quaid-i-Azam University,
Islamabad, Pakistan.

BISMILLAH-IR-RAHMAN-IR-RAHIM

IN THE NAME OF ALLAH, THE MOST GRACIOUS, THE MOST MERCIFUL

Declaration of Authorship

I, MUHAMMAD ALI, declare that this thesis titled, 'Elastic Resonance Scattering Study of Protons on Aluminium' and the work presented in it are my own. I confirm that:

- This work was done wholly or mainly while in candidature for a research degree at this University.
- Where any part of this thesis has previously been submitted for a degree or any other qualification at this University or any other institution, this has been clearly stated.
- Where I have consulted the published work of others, this is always clearly attributed.
- Where I have quoted from the work of others, the source is always given. With the exception of such quotations, this thesis is entirely my own work.
- I have acknowledged all main sources of help.
- Where the thesis is based on work done by myself jointly with others, I have made clear exactly what was done by others and what I have contributed myself.

Signed: _____

Date: _____

Acknowledgements

First of all I would thank Almighty ALLAH and His Prophet (S.A.W.) Whose blessings have been with me throughout my entire life and Whose unlimited blessings made me able to reach this stage of life and complete this thesis.

I feel highly privileged to express my heartiest gratitude to my worthy supervisor **Dr. Sajjad Hussain Bhatti** for his precious time, very kind behavior and continuous guidance throughout this project. It is due to his valuable suggestions and support that helped me to complete this project efficiently. Then I am very much grateful to **Dr. Khunab Gul** for his precious guidance regarding this project. Also special thanks to **Miss Javeria Taj** for her guidance in this thesis preparation.

I am very thankful to **Mr. Muhammad Arif**; Director Experimental Physics Directorate (EPD); for allowing us to avail the accelerator facility and **Dr. Ishaq** and **Dr. Hussnain** for giving adjustments in the time table and other facilities regarding this experiment. Valuable contributions for this experiment were given by **Dr. Faisal**, **Mr. Kashif**, **Mr. Ali**, **Mr. Kamran** and all the staff members in the EPD Accelerator Hall, National Center for Physics (NCP). I am extremely thankful to all of them. I am also very grateful to **Mr. Kashif** and **Dr. Sobia Allah Rakha** for helping me in data analysis.

I am also very grateful to **Dr. Khalid Alamgir** and his research associates at National Institute of Vacuum Science and Technology (NINVAST), NCP for providing us facility of sample preparation. Also special thanks to **Dr. Arshad Saleem Bhatti** Dean Faculty of Science, COMSATS University, Islamabad for providing us the facility of Electron Beam Evaporation System for coating. And I would humbly thank to **Mr. Muhammad Hafeez** and **Mr. Abdul Rehman** at COMSATS University who dedicated their many precious days for the preparation of our samples. I am again very much grateful to both of them.

Finally I feel no hesitation in acknowledging to my family, teachers and all friends for their affections, prayers and care through out my education. I can never forget their endeavor, sacrifice and backup. I have no words for my classmates **Hafiz Ejaz Ahmed** and **Ghulam Farid**. Without them to accomplish this work would never be possible, bundles of thanks to you my friends. May Almighty ALLAH showers His countless blessings on all.

Muhammad Ali

QUAID-I-AZAM UNIVERSITY, ISLAMABAD

Abstract

Faculty of Natural Sciences

Department of Physics

Master of Philosophy

by Muhammad Ali

Proton Elastic Scattering Cross sections have been measured in this thesis for aluminium. The data was collected at two laboratory angles of 140^0 and 170^0. The energy range given was from 1 to 3 MeV in small steps of 0.01 MeV. The aluminium targets were prepared by the deposition of pure aluminium on gold and silver foils which served as backing material. The deposition techniques included Sputtering and Electron Beam Evaporation. The thickness of the coated aluminium target was measured by the resonator of Electron Beam Evaporation System and was about 200 nm. The proton beam used was produced by SNICS-II source and made available by NCP Tandem Accelerator Laboratory, Islamabad. The Non-Rutherford cross sections have been calculated and plotted for both angles. The ratio of Non-Rutherford to Rutherford cross sections have also been calculated and plotted for the same two angles. The results were compared with three past papers of similar calculations and were in qualitative agreement with them.

Keywords: Elastic Scattering, Resonance, (p,p) Reaction, Ion Beam Analysis, Rutherford Back Scattering (RBS), Non-Rutherford Cross Section, Rutherford Cross Section.

Contents

List of Figures

DEDICATED

To

MY BELOVED PARENTS
AND FAMILY

Chapter 1

Introduction

One of the important techniques used for the analysis of light elements in a material is proton backscattering analysis. A proton beam of known energy is incident on the target material and after scattering collected at different angles. The angle at which data is collected is based on the type of technique used. Depending on the energy of incident beam and the nature of target material the interactions are different. At low energy we have atomic interactions resulting in the excitation and de-excitation of atoms. Further increasing energy the ion beam can overcome the coulombic barrier of the atom and interact with the nucleus resulting in the excitation and de-excitation of the nuclear levels.

This thesis deals with the interaction of the proton beam with aluminium nucleus. For the study of light elements in a material lighter beams are best to use. So proton beam is used here which is more sensitive and gives high depth analysis as compared to other beams. The analysis technique used is called Non-Rutherford Backscattering. This technique is used to calculate differential elastic scattering cross sections for aluminium. The experiment is performed at Tandem Accelerator Laboratory of the National Center for Physics (NCP). The results are compared with the experimental data reported in three similar papers, published by different authors.

1.1 History of Scattering Analysis Technique

After the discovery of nucleus by Rutherford, the next task for scientists was to analyze its actual shape and structure. Different techniques were developed and among them the simple and basic technique was that used by Rutherford i.e. to interact charged particles with the given material and analyze the scattered particles. For this purpose an energetic and focused beam was required. The idea of accelerators originated from this point and in 1932 first accelerator was invented by Cockcroft and Walton. Soon some other accelerators were also developed using different mechanisms as that of the first one. Van De Graaf made an accelerator which is still used now-a-days with slight changes in it. The tandem accelerator at NCP is also based on the principle used by Van De Graaf to accelerate charged particles. The decade of 1930 to 1940 is basically the decade of accelerators, in which different accelerators of different energy ranges were developed which paved the way for the scattering studies. So from 1940 onwards, a new era of physics began with the exploration of nuclei of the elements of periodic table. Now every element has been studied through scattering and other techniques and with high energy particle accelerators today, physicists are trying to explore the nucleons.

1.2 Scope of Scattering Analysis Technique

Scattering study played an important role in the analysis of the properties of atoms and nuclei and their energy levels. The improvements in the accelerator technology with the passage of time helped scientists to do experiments with more accuracy and hence more clear and accurate analysis of elements were made possible. Now structure and energy levels either of atom or nucleus are known which contributed a major role in the fields of chemistry and biology. In physics scattering study plays major role in particle physics, nuclear physics and material science. The scattering experiments of particle physics are done at very large energies (from hundreds of MeV to TeV range). Nuclear reactions can take place at relatively lesser energy as compared to particle physics experiments and for material science

experiments even lower energies are required. There are also many industrial applications based on scattering techniques.

Out of different scattering techniques the technique used here is elastic backscattering analysis in which proton beam is back scattered and collected at angles near 180^o. The analysis of the changes in the energy of the backscattered protons and the number of protons backscattered gives us the information about the differential cross section at that specific angle. Physicists have been using this simple technique for over 70 years because it requires energies of the order of a few MeV which is attainable from most of the accelerators present across the world. Our work is also within the energy range of 3 MeV. These moderate energies are sufficient for protons to overcome the coulombic barrier and interact with the nuclei. Then by using the scattering technique the differential cross sections for aluminium nuclei are determined.

1.3 Some Recent Publications on Resonance Elastic Scattering

The elastic scattering technique has been studied over decades and all elements of the periodic table have been analyzed using this technique. This thesis deals with the analysis of nuclear properties of aluminium by calculating differential cross sections for elastic proton scattering. So the publications of elastic proton scattering on Aluminium in the energy range of few MeVs are discussed here.

T. R. Wilkins studied the scattering of protons by magnesium and aluminium up to 6.6 MeV and compared the elastic scattering of protons with Rutherford scattering in 1941. A nuclear scattering camera was used to determine number and energy of scattered protons at different angles between 20^0 and 180^0 [1].

R. S. Bender, F. C. Shoemaker, S. G. Kaufmann and G. M. B. Bouricius studied resonance scattering of protons by aluminium at energies near 985 KeV at 90^0 in 1949. The experimental data was then compared with Breit-Wigner formula [2].

In the energy range of 1.4 MeV to 4 MeV F. C. Shoemaker, J. E. Faulkner, G. M. B. Bouricius, S. G. Kaufmann and F. P. Mooring studied the nuclear reactions resulting from the proton bombardment of aluminium in 1951. The energy dependence of reaction product yields were measured for elastically scattered protons, alpha-particles, gamma-radiation and inelastically scattered protons [3].

Differential cross-sections were measured at 10^0 intervals for the elastic scattering of protons of energy around 10 MeV from eight elements: C, Al, Ni, Cu, Zn, Nb, Ag and Au by G. W. Greenlees, L. Giolietta Kuo and M. Petravic in 1957. Angular range was from 15^0 to 165^0 and the CsI(Tl) crystal detector was used [4].

E. Rauhala in 1989 analyzed the experimental non-Rutherford cross sections at 170^0. Proton backscattering analysis was calculated using Al and Ti. Computer methods were utilized for data analysis and recent work had been checked and updated [5].

In the year 2001 M. Chiari, L. Giuntini, P. A. Mando, and N. Taccetti published their work on proton elastic scattering cross-section on aluminium from 0.8 to 3 MeV and in the angular range from 100^0 to 170^0 in steps of 5^0. A setup for simultaneous many-angle detection of backscattered particles was used [6].

At two angles 140^0 and 178^0 (p,p) elastic differential cross-sections for C,N,O,Al and Si were measured in the energy range of $500 - 2500$ KeV by A. R. Ramos, A. Paul, L. Rijniers, M. F. da Silva and J. C. Soares in 2002. Results were compared with previous data and also the measured cross sections were used to simulate spectra taken from known samples [7].

Finally in the energy interval from 2.4 to 5 MeV Zdravko Siketic, Iva Bogdanovic Radovic, Natko Skukan, Milko Jaksic, and Ana Rita Lopes Ramos measured differential cross sections for elastic scattering of protons from Aluminium at angles of 120^0, 150^0 and 165^0 in 2007. Several resonances were seen with significant deviation from Rutherford value [8].

Chapter 2

Nuclear Theory and Ion Beam Analysis

2.1 Nuclear Reactions

Nuclear reactions can be defined as the interaction of two nuclei, or a nucleon and a nucleus through strong force [9]. A typical nuclear reaction can be described as:

$$a + A \longrightarrow B + b$$

where 'a' is the incident particle , 'A' is the target nucleus which is usually at rest in laboratory frame, 'B' is the residual nucleus and finally 'b' is the ejected reaction product. Usually 'a' and 'b' are nucleons and in some cases are gamma rays. 'A' and 'B' are generally nuclei. Another way of writing above nuclear reaction is:

$$A(a, b)B$$

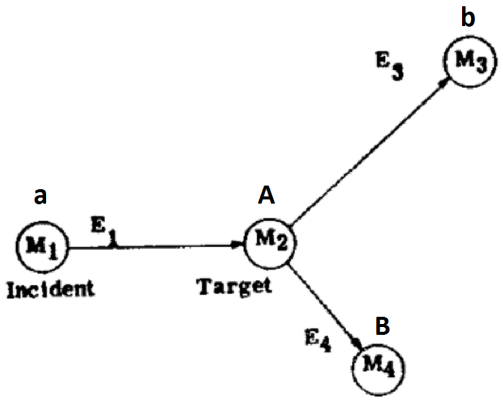

Fig. 2.1: A Typical Nuclear Reaction

For the study of nuclear reactions several conservation laws should be kept in mind:

(1) Conservation of total energy.

(2) Conservation of total linear momentum.

(3) Conservation of total angular momentum.

(4) Conservation of proton and neutron number.

(5) Conservation of parity.

Besides many applications of nuclear reactions study some important uses are: (1) To observe the angular distribution of outgoing particles. (2) To calculate differential, total and absolute cross sections for emitted particles at specific angle and energy. (3) To analyze the spin orientation of different nuclei. (4) To analyze the excited states of nuclei by observing the angular distribution of the γ-radiations.

2.2 Classification of Nuclear Reactions

Nuclear reactions can be classified on the basis of interaction of incoming beam and target nucleus. Nuclear reactions can be classified in three groups: (1) elastic

scattering, (2) inelastic scattering and (3) processes in which one or more nuclear particles or nuclei involved are changed [10].

2.2.1 Elastic Scattering

Elastic scattering between an incident projectile and the target nucleus refers to the reaction in which there is no energy transferred into nuclear excitation. Momentum and kinetic energy of the "system" are conserved but there is usually some transfer of kinetic energy from the incident projectile to the target nucleus. The target nucleus gains the amount of kinetic energy that the incident projectile loses [11].

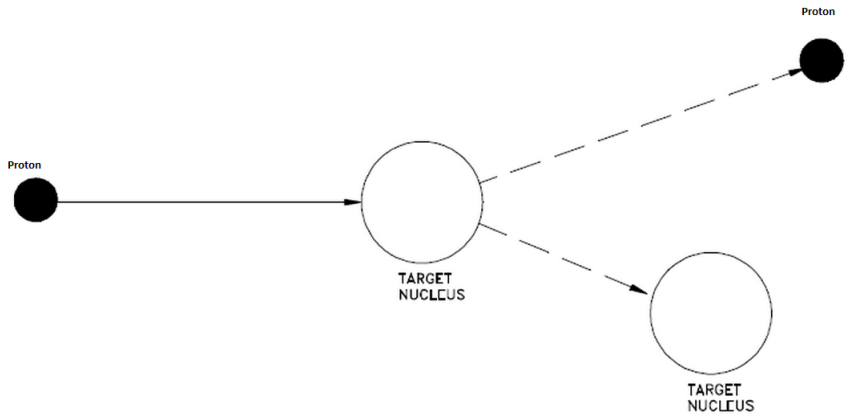

Fig. 2.2: Elastic Scattering of Proton

Elastic scattering can occur in following two different ways:

2.2.1.1 Potential Elastic Scattering

It is the usual elastic scattering in which the incident projectile does not actually touch the nucleus and a compound nucleus is not formed. The incident projectile is actually scattered by short range nuclear forces when it approaches close enough to the nucleus.

2.2.1.2 Resonance Elastic Scattering

It is the interaction in which the incident projectile is absorbed by the target nucleus, forming a compound nucleus, and then the compound nucleus re-emits the same incident projectile in such a way that the total kinetic energy is conserved and the nucleus returns to its ground state. It is dependent on initial kinetic energy of incident projectile. As compound nucleus is formed in this scattering it is also called compound elastic scattering.

2.2.2 Inelastic Scattering

In inelastic scattering, incident projectile is absorbed by the target nucleus to form a compound nucleus. The compound nucleus then emits the same incident projectile with lower kinetic energy and remains in an excited state. Then it usually emits its excess energy through one or more gamma rays to reach its ground state. The sum of kinetic energies of the exit projectile and the target nucleus and the total gamma energy emitted is equal to the initial kinetic energy of the incident projectile.

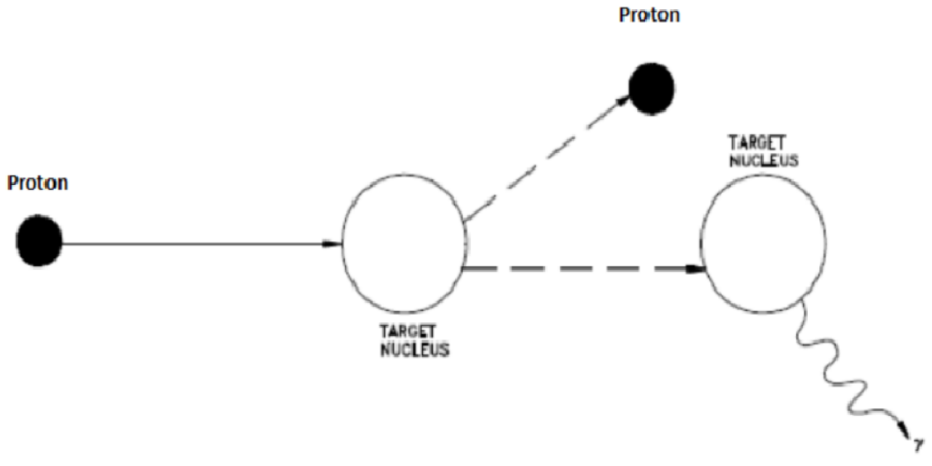

Fig. 2.3: Inelastic Scattering of Proton

2.2.3 Other Reactions

The reactions in which the final particles differ from the initial particles can be divided into six types: [10]

(i) when there is exchange of a proton and a neutron

(ii) the residual nucleus has fewer nucleons than the target nucleus

(iii) the residual nucleus has more nucleons than the target nucleus

(iv) high energy reactions involving mesons, hyperons and heavy leptons

(v) heavy ion reactions using high Z-values beam

(vi) nuclear fission and chain reactions

Some other categories are also useful in the analysis of nuclear reactions besides above classifications. Some of them are discussed below:

2.2.4 Compound Nucleus Reactions

It is the process of compound nucleus formation in which an incident particle is absorbed by the nucleus and shares its energy with few or all particles of the nucleus [10]. The different processes involved are:

(i) re-emission of same species of incident particle with the kinetic energy properties of elastic scattering (compound nucleus elastic scattering) leaving the target nucleus in its ground state.

(ii) re-emission of same species of incident particle with less than the energy characteristic of elastic scattering leaving a target nucleus in excited state (compound nucleus inelastic scattering).

(iii) partial or total de-excitation of the compound nucleus through emission of one of more gamma-rays.

(iv) emission of one or more charged particles or neutrons or both along with the possible emission of gamma-rays.

(v) nuclear fission and heavy ion reactions with the same mechanism as of (iv).

A compound-nucleus theory was proposed by Bohr in 1936. According to this theory the nuclear reaction takes place in two steps: (1) the formation of compound nucleus and (2) the decaying of compound nucleus to final products. The decaying of a compound nucleus is independent of the history of its formation (except in some cases) because the lifetime of the compound nucleus is much greater than the interaction time. Therefore, for the calculation of cross section of a nuclear reaction, one should calculate cross sections of the two processes separately. i.e. The cross section for the formation of compound nucleus and then the decay process (decay process can be treated statistically) [12].

2.2.5 Direct Reactions

A direct reaction is one which proceeds without the formation of a compound nucleus. The time duration of the interaction between incident projectile and target nucleus is very short as compared to the life of a respective compound nucleus. Due to this the reaction products exhibit certain characteristics which are entirely different from those seen if the reaction has proceeded through a compound-nucleus formation. Normally direct reaction interactions have lifetime of the order of 10^{-22} sec whereas the compound nucleus interaction time is typically from 10^{-20} to 10^{-14} sec. The probability of compound nucleus reactions is high at low energies and at high energies direct reactions are more probable. Direct reactions produce more particles at forward angles than expected from a compound nucleus reaction. The examples of direct reactions include inelastic nuclear collision, stripping and its inverse, the pick-up reaction [12].

Besides these reactions there are also other reactions including neutron reactions, fusion reactions, exothermic and endothermic reactions which are characterized differently [10].

2.3 Analysis of Nuclear Reactions

Since the beginning of the nuclear studies, physicists are studying the cross sections and angular distributions of the disintegration products and along with the various theoretical developments, physicists are analyzing the structure of nucleus and the properties of nuclear forces [12]. First, the concept of cross section is discussed here then some nuclear models are described.

2.3.1 Cross Section

The probability of occurrence of a nuclear reaction is conveniently expressed in terms of the concept of cross section. Since interactions in a reaction take place with individual target nuclei independently of each other, it is useful to refer the probability of a nuclear reaction to one target nucleus. Suppose that for each nuclear interaction there is an associated area "σ" such that if the center of the incident particle strikes inside 'σ' a reaction is produced and if the center of incident particle misses 'σ' no reaction is produced. This quantity 'σ' is called cross section and gives a measure of the reaction probability per target nucleus. It is fictitious area which should not be related to the cross sectional area of target nucleus. Mathematically it can be described as:

σ = number of light product particles per unit time, per unit incident flux, and per target nucleus

The unit of cross section is usually 10^{-24} cm^2 or barn [12].

2.3.1.1 Types of Cross Section

In general, a given bombarding particle and target can react in a variety of ways producing a variety of light reaction products. In this case cross section for each interaction (also called partial cross section) is calculated separately and then all partial cross sections are added to calculate the total cross section.

In many nuclear reactions, the light product particles are not produced in an isotropic manner with respect to the incident beam direction. In this case it is useful to define differential cross section "$\frac{d\sigma}{d\Omega}$" in terms of the number of light reaction products "dN" emitted per unit time in a small solid angle "$d\Omega$" at some angle "θ" with respect to the beam. To distinguish σ from $\frac{d\sigma}{d\Omega}$, the cross section σ is sometimes called an integrated cross section i.e.:

$$\sigma = \int_{allspace} \frac{d\sigma}{d\Omega} d\Omega \tag{2.1}$$

The aim of any theory of nuclear reactions is to explain the energy and angular dependence of cross sections in terms of certain nuclear parameters. An example is **Coulomb or Rutherford Cross Section** in which elastic scattering of low energy charged particles by coulomb forces is studied. Another example is **Non-Rutherford Cross Section** in which resonance elastic scattering of charged particles by nuclear forces is studied.

2.4 Nuclear Models

Soon after the discovery of nucleus, the shape and properties of nucleus, forces present between nucleons and their interactions were to be analyzed by physicists. In this aspect various models and calculations were done by different physicists but unfortunately no model has described the nature of nucleus completely. Every model has its limitations and agrees with the experimental results in a certain domain or under certain approximations or assumptions. Some of the nuclear models are discussed here.

Liquid Drop Model is one of the earliest models which discussed the binding energy of nucleus in accordance with the experimental results. Nucleus was considered an incompressible liquid droplet with nucleons playing the role equivalent to molecules in a drop of normal liquid. The individual quantum properties of nucleons were completely ignored [13].

The Fermi-Gas Model was also one of the earliest models and it included quantum mechanical effects in analyzing nuclear structure contrary to the liquid drop model. The nucleus was treated as a gas of free protons and neutrons confined in a very small region of space called nuclear volume. The nucleons were expected to have discrete energy levels within the nucleus. Nucleus was considered similar to a spherically symmetric well. The protons and neutrons were considered to have their own corresponding levels [13].

Nuclear Shell Model is based on the theory of atomic physics. All the properties of atoms such as energy levels of electrons, their different quantum numbers (n, l, m_l, m_s), degeneracy properties etc. were applied to nucleons and the nucleus (spherical) as well in a similar manner as that of atom. The mean potential for nucleons was assumed to be central and nucleons were assumed to be moving in this potential. This model was applied to both single particle and many body treatment. This model was a big success in explaining nuclei but it failed to explain many excited levels of nucleus and their dipole and quadrupole moments [13].

The Unified Model was developed by Bohr. It is a combination of liquid-drop model and shell-model with certain differences. The shell model potential was assumed to be non-spherical and the nucleons were assumed to move approximately independently rather than being strongly coupled as in the case of liquid-drop model. The unified model explained vibrational and rotational excitations and spectra [12].

The Collective Model was developed by Bohr, Mottelson and Rainwater. The nucleus was assumed to have a hard core of nucleons in the filled shells and the outer valence nucleons were assumed to behave like the surface molecules in a liquid drop. The nucleus was considered non-spherical (ellipsoidal oblate and prolate). It explained the dipole and quadrupole moments of the nuclei and also rotational and vibrational excitations. The unified and collective models are often treated as a single **Unified (Collective) Model** [13].

The Optical Model was developed by Feshbach, Porter and Weisskopf in 1949 which represents the nucleus by a complex potential called optical potential. The imaginary part of the potential accounts for the inelastic processes. The Schrodinger equation when solved for the optical potential, being a function of space coordinates and energy of the bombarding particle, gives the scattering and reaction cross sections. The optical model is the analogy of the scattering of light by a refracting and absorbing medium using a coupled refractive index [14].

2.5 Ion Beam Analysis

Ion Beam Analysis (IBA) is the study of the interaction of an incident ion beam with a specific target material and it refers to all the techniques which can be utilized for a particular analysis of an experiment. The accelerator gives an intense and focused beam. So due to the energy and nature of the ion beam, the interactions of the ion beam with the target material can be different depending upon the geometry of the material, ion beam and detector. The most common techniques used are RBS, ERDA, PIXE, and NRA which are discussed below.

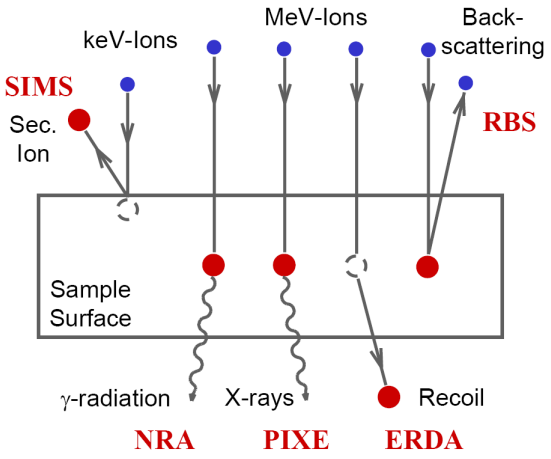

Fig. 2.4: General Ion Beam Analysis Techniques

2.5.1 Rutherford Backscattering RBS

Rutherford Backscattering is the analytical technique which uses accelerators. It is based on the detection of charged particles elastically scattered by the nuclei of the target sample. The energies of these backscattered particles are measured. The analysis of energy losses in collision with the atomic nuclei depends upon the atomic number Z of each element present in the sample. Hence by analyzing energy losses the qualitative as well as quantitative analysis can be done without standards. It is basically elastic nuclear collision and conservation of energy and momentum holds. It is an important tool for material analysis and give depth distribution of the impurity elements in parts per million range in thin surface region of the sample. The fundamental uses of RBS are: [15]

- Species Analysis (through Kinematic Factor 'k')
- Concentration of Species (through Scattering Cross Section 'σ')
- Depth Profiling (through Energy Loss or Stopping Power 'S')

In our work Rutherford and Non-Rutherford Cross sections have been measured in the laboratory frame of reference. Rutherford scattering cross section σ in the laboratory frame of reference is given by the relation:

$$\sigma_R(E,\theta) = \left(\frac{Z_1 Z_2 e^2}{16\pi\epsilon_0 E}\right)^2 \frac{4}{\sin^4\theta} \frac{\left[\sqrt{1-(\frac{M_1}{M_2})^2\sin^2\theta}+\cos\theta\right]^2}{\sqrt{1-(\frac{M_1}{M_2})^2\sin^2\theta}} \tag{2.2}$$

where

σ_R corresponds to Rutherford cross section in cm^2 or barns per steradian

Z_1 and Z_2 are the atomic numbers of protons(incident) and Aluminium(target)

M_1 and M_2 are the masses of protons(incident) and Aluminium(target)

E is the energy of incident beam in MeV

θ is the scattering angle

A schematic diagram of Rutherford technique is shown in fig. 2.5.

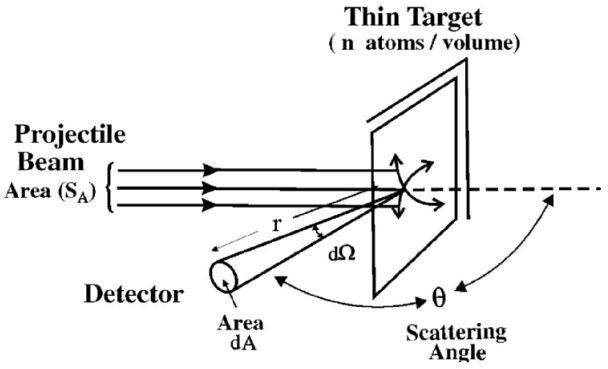

Fig. 2.5: Rutherford Back Scattering

When energy of incoming particle increase nuclear forces come into play and in calculations these are included. This is the case we are dealing with in this thesis and it usually happens when the energy of incident beam is high, scattering angle is high and the respective target elements are light elements. In such cases cross section is named as Non-Rutherford Scattering and this Non-Rutherford cross section deviates from Rutherford cross section due to involvement of nuclear forces because the distance of closest approach decreases to the nuclear size. There can be elastic or inelastic scattering for Non-Rutherford cross section but it has been observed that at resonances the Non-Rutherford elastic cross section becomes several times greater than that of Rutherford elastic cross section. Hence the resonance points are of great importance in the analysis of specific nuclei. We are also interested in such points. The Non-Rutherford Elastic Cross section is given by the following relation:

$$\sigma = \frac{d\sigma}{d\Omega} = \frac{1}{nt}\frac{1}{d\Omega}\frac{dQ}{Q} \tag{2.3}$$

where

σ corresponds to Non-Rutherford cross section in cm^2 or barns per steradian

Q is Number of particles that have hit the target

dQ is Number of particles recorded by the detector

n is volume density of atoms of the target element

t is the thickness of the target element

$d\Omega$ is the solid angle subtended by the target on the detector

n and $d\Omega$ are given by the relations:

$$n = \frac{N_A \rho t}{M} \tag{2.4}$$

$$d\Omega = \frac{dA}{r^2} \tag{2.5}$$

where

N_A is the Avogadro Number

M is the molecular weight

ρ is the bulk density in grams per cubic cm

ρt is the mass areal density

dA is the area of detecting surface of the detector

r is the distance between the target element and the detector

2.5.2 Other Techniques

NRA - Nuclear Reaction Analysis is a nuclear method for material characterization. The ion beam particles interact with the nuclei of the target material and leave them in excited state under resonance conditions. On decaying, the nuclei emit the amount of energy absorbed and the emitting radiation is detected. So by

detecting the intensity of the radiations emitted, the concentration of the target atoms can be measured.

ERDA - Elastic Recoil Detection Analysis is also used for measuring concentration of light elements in a material. The basic principle is elastic nuclear reaction between a relatively heavy ion beam and the light elements in the target material. The heavy ions of beam recoils the lighter elements in the target and fill their places by themselves. Detectors are attached which measures the concentration of light elements kicked out. It is a powerful tool to trace hydrogen in materials.

PIXE - Particle Induced X-ray Emission is a technique which uses X-ray emission for elemental analysis. The incoming ion beam excites the inner-shells of the target material's atoms which upon de-excitation emits X-rays which are detected and hence the different elements can be analyzed. This technique is basically not a nuclear technique because it is the interaction of ion beam with atomic levels not the nucleus.

Chapter 3

Experimental Setup

The main apparatus used for the experiment is Tandem Pelletron Accelerator which is discussed later. First the accelerators are generally discussed. The main job of an accelerator is to accelerate charged particles and thus obtaining an intense beam of known energy and intensity. For this purpose several accelerators have been constructed since $1930's$. Depending on the working principles, accelerators can be categorized as Electrostatic Accelerators and Resonance Accelerators. The main difference between them is that electric field is constant in the former and variable in the later case. The electrostatic accelerators use direct voltage acceleration and include Cockcroft Walton accelerators, Van de Graaff accelerators, Pelletron Single Ended accelerators and Pelletron Double Ended (Tandem) accelerators. Cockcroft Walton used HV (High Voltage) capacitors and HV rectifiers to accelerate charged particles. Van de Graaff used mechanical method to transfer charged particles from one end to another and this technique was enhanced in later accelerators. Resonance accelerators used variable electric fields and includes Linear Accelerators and Cyclic Accelerators which further includes Betatrons, Cyclotrons and Synchrotrons. The accelerator available for our experiment was Pelletron tandem accelerator at National Center for Physics (NCP) [16].

3.1 Pelletron Tandem Accelerator

A tandem accelerator uses the basic principle of Van de Graaff Electrostatic Accelerator. Van de Graaff used insulator belt to move electric charges to a HV(High Voltage) terminal. The charges are generated at one end by field effect from a comb and extracted in a similar way at the other end. The HV is distributed along the column through a resistor. To overcome the difficulties in this mechanism Raymond Herb in 1965 changed the charging belt from a continuous smooth belt to one with steel cylinders held apart by nylon insulating links in the form of a chain. Herb named machines using these belts pelletrons and these machines were called pelletron single ended accelerators. Then in order to attain more ion beam energy from the single HV terminal, another mechanism was introduced which is used in our accelerator. In this mechanism negative charges are generated from one end, attracted by the central HV terminal and after reaching this central HV terminal the charges are converted into positive ones through stripping and hence these charges(or beam) are again made to move away from the central potential and accelerate towards the other end. Both ends are usually at ground and the beam or charges gains the energy twice as that of pelletron single ended accelerators. Hence these accelerators are named as Pelletron Double Ended Accelerators or Tandem Accelerators. The energy ranges are a few MeVs depending upon the type of beam used [16].

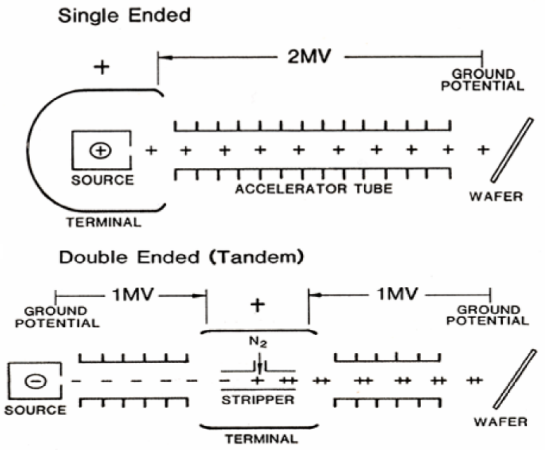

Fig. 3.1: Single and Double Ended Pelletrons System

3.2 5-UDH Pelletron Tandem Accelerator

The accelerator at NCP is 5-UDH Pelletron Tandem Accelerator. Its basic principle is discussed above. The basic components of this accelerator are:

- Ion Sources
- Ion Beam Transport and Focusing Components
- Accelerator Tank
- End Stations

The details about these components are given below:

3.2.1 Ion Sources

As stated earlier the main job of an accelerator is to accelerate charges. So initially some charged particles of less energy are required for the accelerator which should be given to one end of the accelerator to accelerate them. For this purpose ion sources are used. Ion sources produce ions from neutral atoms through different techniques depending on the type of ion source used. The aim is to produce a stable and intense beam of desired charges. The ion source is either connected directly to the acceleration tube entrance or it is placed separately near ground potential with small potential difference in order to give the ions some acceleration. Two ion sources are used in NCP which are placed near ground potential and are discussed below.

3.2.1.1 RF Ion Source

RF (radio frequency) ion source produces positive ions. A neutral gas is sent into the quartz bottle through gas cylinders as shown in fig. 3.2. It is called an RF ion source because it dissociates the neutral gas through an RF oscillator which is

connected to the quartz bottle. Ions are pushed out of this chamber by applying small potential at the ends. Positive ions are produced through this process which can also be converted to negative ions (if needed) by injecting them to a rubidium charge exchange cell. Molecular, singly and doubly charged ions can be produced by this process. Normally heavy ions are generated from this source. In NCP mostly helium beam is generated from this source [17].

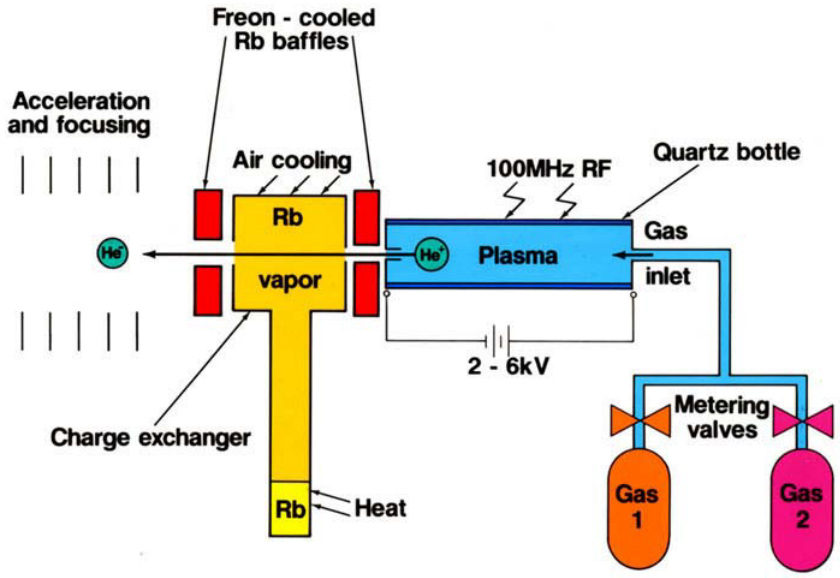

Fig. 3.2: Sketch Diagram of RF Ion Source

3.2.1.2 SNICS

The Source of Negative Ions by Cesium Sputtering (SNICS) produces a negative ion beam. As shown in fig. 3.3, there is a cooled cathode and heated ionizing surface. Cesium vapors from the cesium oven are brought in the region between cathode and ionizing surface. Some of them condenses on the front of cathode and some are ionized by ionizing surface and these ionized charges are attracted by cathode, sputter particles there and as a result pick up electrons through the condensed cesium layer producing negative ions. For tandem accelerator we require a negative ion beam at its entrance which can be achieved directly from negative ion source or by positive ion source followed by a charge exchanger. Tandem

accelerator at NCP has double injection entrance; RF source for light ions and SNICS for heavier and metal ions [17].

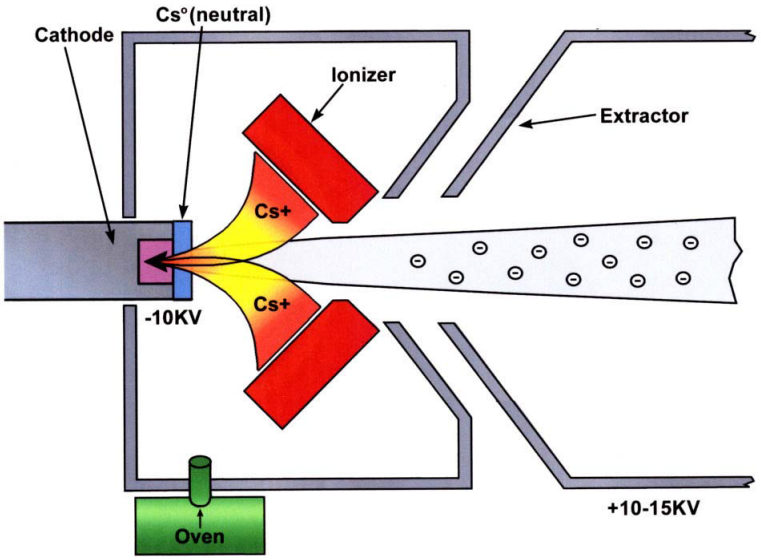

Fig. 3.3: Sketch Diagram of SNICS Ion Source

3.2.2 Ion Beam Transport and Focusing Components

3.2.2.1 Beam Selection

Soon after the extraction of ions it is required to obtain a beam of specific charged particles. The ions extracted may contain several types of charged particles. For this purpose a filter is placed after the ion source and before the accelerator tank which uses orthogonal electric and magnetic fields. The fields are adjusted so that the desired beam components pass without any deflection and other undesired components are deflected away [17]. For zero deflection we have the equation:

$$v = \left(\frac{2E_1}{M}\right)^{\frac{1}{2}} = \frac{E}{B} \tag{3.1}$$

where

E_1 is the energy of the beam

M is the mass of ion

E is the electric field

B is the magnetic field

Only those species pass through these orthogonal fields whose velocity is equal to "$\frac{E}{B}$", while other species are deflected. Hence the undesired ions are filtered out by this **Injector Magnet**.

Analyzer Magnet is used for energy stabilization. It is actually a dipole magnet and it is also used for beam focusing and deflection. Dipole magnet differentiates charges on the basis of their "$\frac{e}{m}$" ratio hence several charges are differentiated mainly due to their different masses by dipole magnet.

Then to separate the charges on the basis of their charges only we use **Electrostatic Analyzer** or **Enzel Lens**. They also focus the beam towards the terminal stripper into the accelerator tank. These is done by passing the ion beam through static electric fields. A diagram below (fig. 3.4) shows an Electrostatic Einzel Lens.

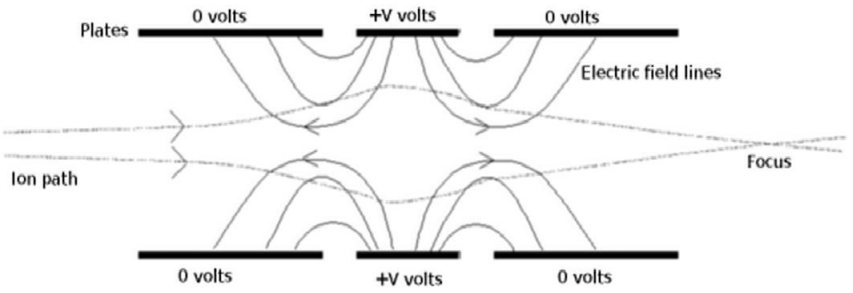

Fig. 3.4: Einzel Lens

3.2.2.2 Beam Collimation

The beam selected above should have a well defined shape and size because it can diverge and hence intensity and shape of the beam could not be accurate. First the beam is defined only in the horizontal plane by **Analyzer Slits**. This prevents the divergence of the beam in the vertical plane and keeps the beam on track. These consists of two stainless steel slits which are movable electronically in micrometers range [17].

3.2.2.3 Beam Transport and Focusing

To get a well defined and intense beam it is required to move the beam well focused and convergent. For this purpose **Magnetic Quadrupole** and sometimes **Electrostatic Lenses** are used. Usually magnetic quadrupole is used at high energy. It has three coils. First focuses the beam along x-axis, second along y-axis and third again along x-axis [17]. Other components used for beam transport are discussed in the preceding paras.

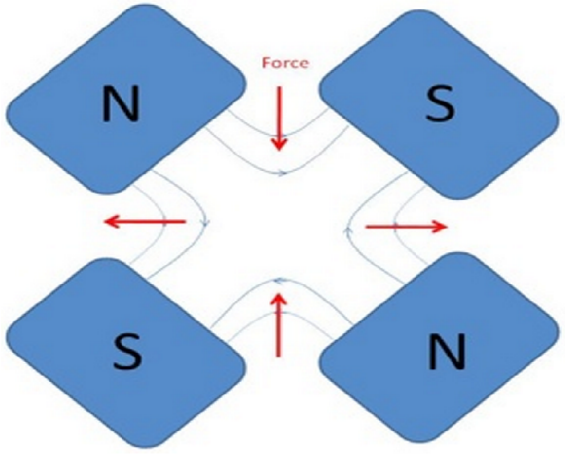

Fig. 3.5: Magnetic Quadrupole Lens

Beam Profile Monitors (BPM) is used to check the shape and intensity of beam in the X-Y directions. The BPM used in NCP is NEC Model BPM-8. These are located at different positions along the beam lines. **Beam Line Valve (BLV)** is used to stop the beam at appropriate points along the beam line. **Faraday Cup (FC)** is used to measure beam current at several places. It can also be used to stop the beam at the points where FC is placed along the beam line [17].

Apertures or Slits are used to define the size of the beam at the entrance and exit of the analyzer magnet and before the samples. **Electrostatic X-Y Steerer** contains two orthogonal plates for accurate, low power electrostatic steering of charged particles. It can also deflect beam by supplying high voltages to the plates. **High Energy Beam Line** is the region where we have a high energy beam moving. Normally it is after the main terminal at the accelerator tank

and this line requires extra care. For focusing magnetic quadrupole triplet lens is used followed by a magnetic Y-steerer and the analyzing magnet. At the end of high energy beam line there is an analyzing magnet equipped with seven ports at $\pm 45^0, \pm 30^0, \pm 15^0$ and 0^0 with respect to the accelerator [17].

Towards the endstations there are two **Extended Beam Lines** at the NCP accelerator. One is at 15^0 for material science analysis and other is at 30^0 for nuclear physics experiments. A single slit followed by a matched set of two slits to control the divergence of the ion beam, a quadrupole doublet magnet, X-Y steerer, a FC and a BPM all are equipped with these beam lines. Despite these there is also room for more beam lines but presently there are only two beam lines [17].

3.2.3 Accelerator Tank

The whole mechanism of acceleration is contaminated inside a tank in order to prevent environmental effects. The accelerator components are provided a vacuum environment within the tank and furthermore the ion beam moving inside the tank is given an ultra high vacuum beam line path inside the tank. The main components in an accelerator tank are Enzel Lens; Insulating Column consisting of 10 modules of 1 MeV each; High Voltage Terminal; Stripper along with two small turbo pumps for circulating stripper gas; Charging System; Generating Voltmeter (GVM); Two Capacitive pick offs; and Corona Probe. The negative ions from the ion sources enters the accelerator tank through Enzel lens. These negative ions are attracted by the central high terminal voltage. Hence these ions accelerates towards the central potential till they reach there. A stripper foil (either thin film or some gas) is placed at this terminal which stripes the negative charges to convert them to positive charges which are then repelled by the same high potential and hence the charges reach the high energy beam line to move towards the extended beam lines.

3.2.3.1 Charging System

As discussed earlier tandem accelerator uses pelletron charging system for charging. Pelletron are made of metal pellets and interconnected by insulating nylon links. These are charged through induction scheme. For the central potential to be positive, negatively charged inductor electrodes are used to push the electrons off the pellets. This is done when the pellets are in contact with the drive pulley which is at ground potential. The pellets being in range of the inductor field gets positively charged and the chain moves this charge to high terminal where reverse process takes place. The terminal inductor electrodes are given voltages by drawing a tiny amount of charge from the chain. The system can deliver $100 - 200$ μA or more per chain to the high voltage terminal [17]. The schematic diagram is shown in fig. 3.6.

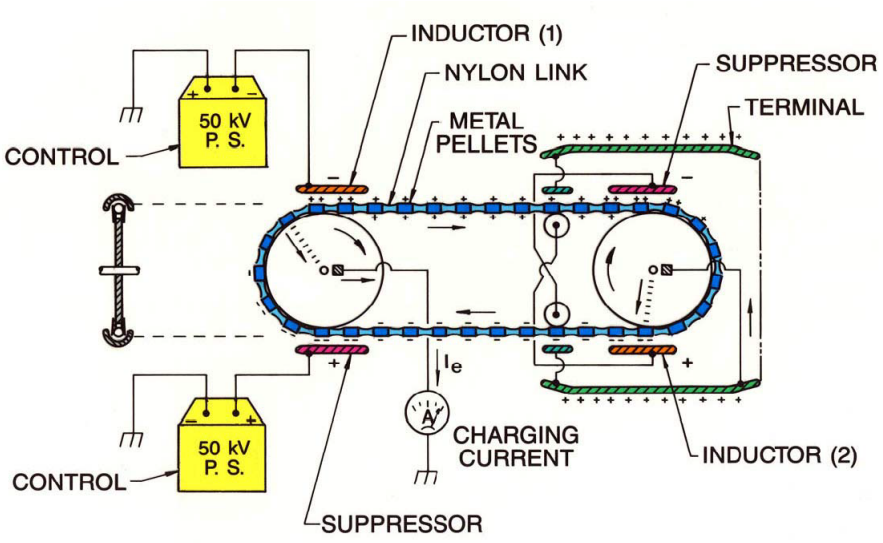

Fig. 3.6: Pelletron Charging System

3.2.3.2 Corona Pobe System

It consists of sharp needles and placed near terminal. These are used to reduce the excess of charge if required. It is brought to the place where charges had to be reduced and the charges flow through its needles and are grounded. Hence voltage stresses are relieved. There are several corona points within the accelerator tank

through which the peak stress of voltages is decreased in a control manner. Hence the probability of a spark is greatly reduced.

3.2.3.3 Stripping System

The conversion of negative ions to positive ions is done by stripping electrons from negative ions by a target medium in the high voltage terminal of the tandem accelerator. There are two types of charge exchange processes Electron Capture and Electron Loss. Generally the change of ion charge state is the consequence of multiple combination of these two fundamental processes.

3.2.3.4 Insulating Gas

Dust, foreign bodies and especially metallic particles can all initiate breakdown. To avoid this SF_6 gas is used as an insulating medium. The gas is continuously recirculated through a tube from its own tank situated adjacent to accelerator tank in a separate room. Recirculation helps to remove moisture and secondary products.

3.2.3.5 Generating Voltmeter (GVM)

An electrical circuit called stabilizer is used to stabilize the terminal voltage. It is a feedback circuit and operates in two modes namely Generating Voltmeter (GVM) and Slit Control. In GVM the terminal voltage is measured by Generating Voltmeter and compared with the terminal voltage specified by the experimenter and the difference is adjusted by stabilizer via corona tube grid biasing.

3.2.3.6 Vacuum System

In order to get accurate results the whole system including the ion sources, accelerator tank, beam lines and target chambers should be kept in vacuum. For

this purpose several pumps are attached with the system at different places. Ion sources and all beam lines are vacuumed by Turbo and Rotary Pumps. Base pressure in low energy beam line is about 10^{-8} Torr and in high energy beam line is 10^{-9} Torr. To measure the pressure at different places three gauges are attached. The target chambers have separate vacuum pumps attached specifically to chambers only in order to maintain the vacuum of ion beam lines. Apart from these there is also cooling system for high voltage devices which includes pump, air cooled heat exchanger, a fan, a fluid reservoir etc.

3.2.4 Endstations

The 5MV Tandem Accelerator at NCP has two end stations with respect to the beam line.

- NEC RC43 Analytical Endstation
- NEC RS61 Scattering Endstation

Fig. 3.7: Endstation at NCP

3.2.4.1 NEC RC43 Analytical Endstation

This endstation is used for material science analysis and it has a computer controlled system including sample holder. It is attached to 15^0 beam line. It has the options of sample movement about the beam and also detector movement. Also the more accurate sample adjustment can be done by computers using CCD camera. The computer software controls 4 MCA (Multi-Channel Analyzer) data collection cards and the techniques used are: Rutherford Backscattering (RBS), Elastic Recoil Detection (ERD), Nuclear Reaction Analysis (NRA), Particle Induced X-Ray Emission (PIXE) and channeling. The softwares used for these techniques includes RUMP for RBS, Non-RBS and ERD anlysis; GUPIX for X-ray spectrum or PIXE analysis; and SIMNRA for NRA [17]. The detectors attached to the chamber are:

- Fixed Ion Detector at 170^0 for RBS
- Movable Ion Detector ($0^0 - 80^0$) for grazing-angle scattering
- Scintillation NaI(Tl) Gamma-Ray Detector for NRA of light elements
- Retractable SiLi X-ray Detector for PIXE analysis of trace elements

For the measurement of differential cross sections the detectors used are fixed ion detector and movable ion detector. Both of them are Silicon Surface Barrier Detector.

3.2.4.1.1 Silicon Surface Barrier Detector

It is a charged particle detector formed by high purity n-type silicon wafer. One side of the wafer is chemically etched and a p-layer is formed via spontaneous oxidation and further a thin gold layer is evaporated on this layer for contact. When reverse biasing is applied a high-resistance depletion region is formed. Electron-hole pairs produced by a charged-particle in this region give rise to an output signal which is dependent on the kinetic energy of incident charged-particle. For an output signal the detector must have a depletion region thick enough to stop

the particle completely. The energy resolution of the surface-barrier detector is a function of the energy of the incident charged particle and is also affected by the noise from the signal amplification electronics and the detector. The energy resolution of these detectors is about 15 keV [15].

3.2.4.2 NEC RS61 Scattering Endstation

It is connected with the 30^0 beam line extension. It is used for nuclear reaction analysis and experiments. The chamber has two surface barrier detectors capable of moving. Several techniques used by this end station includes interface analysis, defects quantification, high-energy ion implantations and light element quantification using ERDA and NRA in the materials. The experiment for the measurement of differential cross sections was to be done on this endstation but due to non-availability of this endstation our experiment was done on other endstation.

Chapter 4

Data Collection and Analysis

The lab facility of 5MV Tandem Accelerator was provided by National Center for Physics EPD lab. The experiment was carried out in collaboration with the operating staff. The experiment details are given below:

4.1 Sample Preparation

First the sample holders were prepared. Thin aluminium sheets were purchased commercially and cut into small circular discs of approximately 1 inch diameter. Then two small holes at the top and one big hole at lower center of the disc were made by drilling. The small holes were made to connect the sample holder with the holder at the target chamber of the accelerator and the big hole of approximately 8 mm diameter was made to place our target material and expose this target material to the incoming incident beam. Thin gold and silver foils in microns thickness were purchased commercially and were stuck at the big hole with the help of very thin carbon double tapes and some foils were stuck using small amount of glue. The foils were stuck in such a way that they had a contact with the sample holder either directly or through carbon conducting tape.

The samples were kept in an air tight commercially purchased desiccator with some amount of silica gel to absorb moisture. Then the required pure aluminium

layer of 170 - 200 nm were coated on these samples using electron beam evaporation system. The electron beam evaporation facility was provided by COMSATS university. The pure aluminium was provided by NINVAST at National Center for Physics. In this way pure aluminium layer in nm thickness was coated on gold and silver foils and the samples were ready to be exposed by the ion beam.

4.2 Endstation

The scattering chamber used was 15^0 NEC RC43 Analytical Endstation. The chamber has its own vacuum system and controlling apparatus. It is manually controlled at the accelerator hall. The sample are placed at the holder in this chamber but first the lid of the chamber is opened after venting the whole chamber. The holder rod can be brought out of the chamber for placing the sensitive target on it. The rod is attached at the front of the incoming beam line. After placing the sample on this holder and adjusting the detector position the chamber lid is closed.Then initially rotary and then turbo pump is started for vacuuming. The interior diagram of the chamber is shown in fig. 4.1.

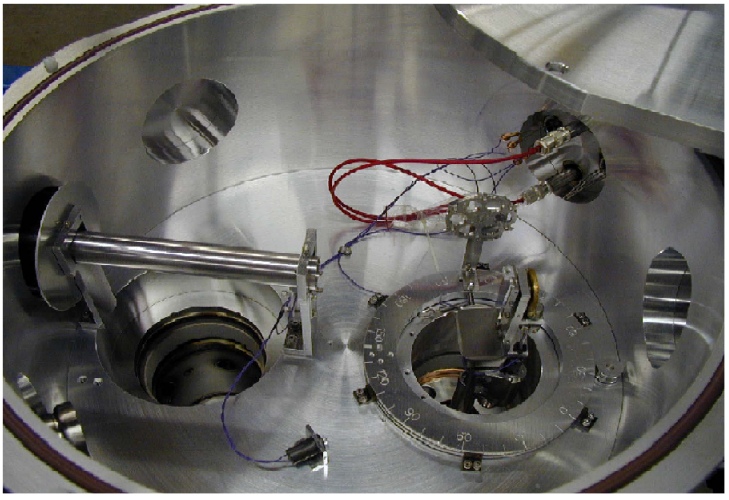

Fig. 4.1: Interior Diagram of 15^0 Endstation

The sample position can also be checked via a small glass window at one end of the chamber and also the detector position can be changed from outside without

disturbing the internal vacuum. The sample position is adjusted accurately by the computer system installed in the operating room. The x, y and z-axis can be changed with high accuracy in order to expose the sample exactly at front of the incoming ion beam. After vacuuming the incident beam line valve is opened and the experiment is ready to begin.

4.3 Detectors

The two detectors used for the counting of the scattered particles are silicon surface barrier detectors. One detector is fixed at 170^0 and mainly used for RBS analysis. It is at a distance of 13.5 cm from the target. Other detector is placed on a 15 cm diameter circle on which angles are calibrated. It is a movable detector and can be adjusted to any particular angle of scattering. The movable detector is at a distance of 7.5 cm from the target, and is placed at the center of the circle on which detector is placed. In our experiment we adjusted the movable detector at 140^0. The diameter of surface area of both detectors exposed for the detection of charges is 5.5 mm. The detectors are ORTEC silicon surface barrier detectors. The coming signal from the surface barrier detector (SBD) is proceeded to Canberra 2003BT preamplifier, then it goes to CANBERA spectroscopy amplifier and then to ORTEC ADC and finally to multi channel analyzer (MCA). The detectors are connected with the computers at the control room where the data is collected by different softwares depending on the analysis technique used. A schematic diagram of data collection process is shown in fig. 4.2 :

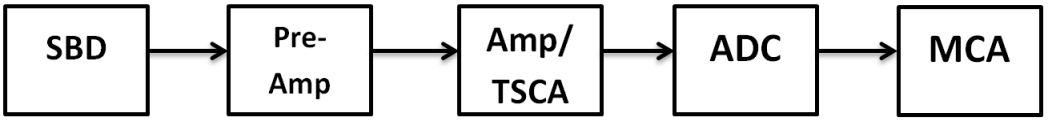

Fig. 4.2: Electronics Circuit Diagram of Data Collection Mechanism

4.4 Experimental Procedure

After the installation of the sample at the endstation the experiment was carried out. The proton ion beam was generated from the SNICS source. The different components discussed before gave the information about the beam's intensity and dynamics and finally a well focused ion beam was hit on our target at the 15^0 endstation. The energy of the incident beam was varied from 1 MeV to 3 MeV in small intervals of 0.01 MeV. The intervals were given by the controller. The charge collection was set at 10μC by the RUMP software installed on the computers connected with the MCA cards of the detector. The data was collected by this software for each interval and stored in computers. The graphs were plotted for each interval showing channel numbers on x-axis and number of counts on y-axis. The channels were calibrated with energy so the graphs showed the energy vs counts readings. A typical graph is shown in fig. 4.3 :

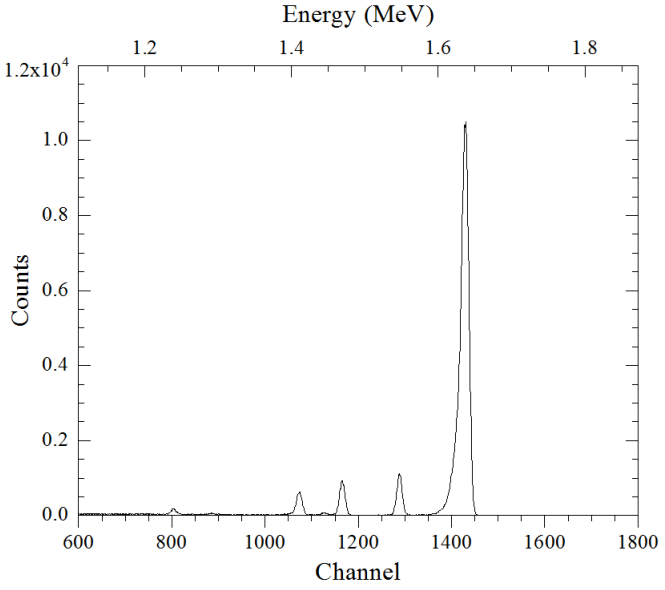

Fig. 4.3: A Plot of Data on RUMP Software

Some initial readings were checked as whether the graphs show proper signals of the different elements of the target sample and whether there is some background noise or not. Background noise was reduced by shielding the detector when required otherwise we got good graphs and readings for the experiment. The graphs showed

peaks of gold, aluminium, carbon and oxygen etc. Data at each step was collected manually using the software. Both detectors were used separately i.e. when 170^0 detector was used then 140^0 detector was switched off and vice versa. In this way data was collected and analyzed using RUMP software which gave counts at every energy step.

4.5 Data Analysis

The Non-Rutherford Differential Cross Section (eq. 2.3) is calculated by:

$$\sigma = \frac{d\sigma}{d\Omega} = \frac{N_{peak}}{d\Omega N_t N_{incident}} \tag{4.1}$$

where

N_{peak} is the total number of counts in a respective peak

$N_{incident}$ is the total number of incident particles (protons)

dΩ is the solid angle of the detector used

N_t is the number of target atoms per unit area (areal density)

"$N_{incident}$" is calculated by the formula:

$$N = \frac{Q}{e} = Q(6.25 \times 10^{12}) \tag{4.2}$$

"Q" represents total charge collected by the faraday cup in μC which was set at 10 in our experiment and 'e' represents charge on a single proton. "N_t" is calculated (eq. 2.4) by the following formula:

$$N_t \left(\frac{atoms}{cm^2}\right) = \frac{\rho_A \left(\frac{g}{cm^2}\right) N_A \left(\frac{atoms}{mole}\right)}{A \left(\frac{g}{mole}\right)} \tag{4.3}$$

"ρ_A" is areal density of the target, 'N_A' is avogadro number and 'A' is the atomic mass of the target. Finally the solid angle $d\Omega$ is calculated (eq. 2.5) by the formula:

$$d\Omega = \frac{A}{r^2} = \frac{\pi R^2}{r^2} \tag{4.4}$$

where 'A' is the front area of the detector in mm^2 exposed to the particles for detection, 'r' is its distance from the target in mm and 'R' is the radius of the detector front area in mm. For the movable detector at 140^0 $r = 75mm$ and $R = 2.75mm$ hence its solid angle becomes:

$$d\Omega = \pi \left(\frac{2.75}{75}\right)^2 = 0.00422sr$$

Similarly for the fixed detector at 170^0 $r = 135mm$ and $R = 2.75mm$ hence its solid angle becomes:

$$d\Omega = \pi \left(\frac{2.75}{135}\right)^2 = 0.0013sr$$

Substituting above values in the main equation 4.1 and simplifying the equation for the movable detector, it becomes:

$$\sigma\left(\frac{barn}{sr}\right) = \frac{d\sigma}{d\Omega} = 6.293 \times 10^{-11} \frac{AN_{peak}}{Q\rho t} \tag{4.5}$$

and similar calculations for the fixed detector gives:

$$\sigma\left(\frac{barn}{sr}\right) = \frac{d\sigma}{d\Omega} = 2.0388 \times 10^{-10} \frac{AN_{peak}}{Q\rho t} \tag{4.6}$$

where 't' is the thickness of the coated layer of Al and ρ is its volume density.

The Rutherford Cross section (eq. 2.2) is also calculated by:

$$\sigma_R(E,\theta) = 0.02073 \left(\frac{Z_1 Z_2}{4E}\right)^2 \left[\left(\sin\frac{\theta}{2}\right)^{-4} - 2\left(\frac{M_1}{M_2}\right)^2\right] \tag{4.7}$$

Hence Rutherford Cross Section (σ_R), Non-Rutherford Cross Section (σ) and their corresponding ratios $\frac{\sigma}{\sigma_R}$ are calculated and the results are plotted.

Chapter 5

Results and Discussions

5.1 Experimental Results

Rutherford and Non-Rutherford elastic scattering cross sections of protons from aluminium at two different angles of 140^0 and 170^0 have been measured experimentally using proton beams of different energies. Figures 5.1 and 5.2 show graphs of Non-Rutherford cross sections versus energy at 140^0 and 170^0, respectively. Figures 5.3 and 5.4 are the graphs of ratio of Non-Rutherford to Rutherford cross-sections versus energy at 140^0 and 170^0, respectively. In the energy range used in these experiments, the Non-Rutherford cross section curves and ratios of Non-Rutherford cross-section to Rutherford cross-section excitation curves are not smooth. Sharp peaks represent the resonances of the proton-target system. In figures 5.1 - 5.4 we can observe these peaks. The spectrum at 140^0 shows narrower resonances than at 170^0. The threshold energies for resonance proton scattering by aluminium through smaller scattering angles are higher. For the angular range $160^0 \leq \theta \leq 180^0$, the proton energy at which cross sections deviate from Rutherford values by >4% is found to be consistent with,

$$E_{lab}^{NR} = (0.12Z_2 - 0.5)\text{MeV}$$

within accuracy of ± 0.5 MeV [18].

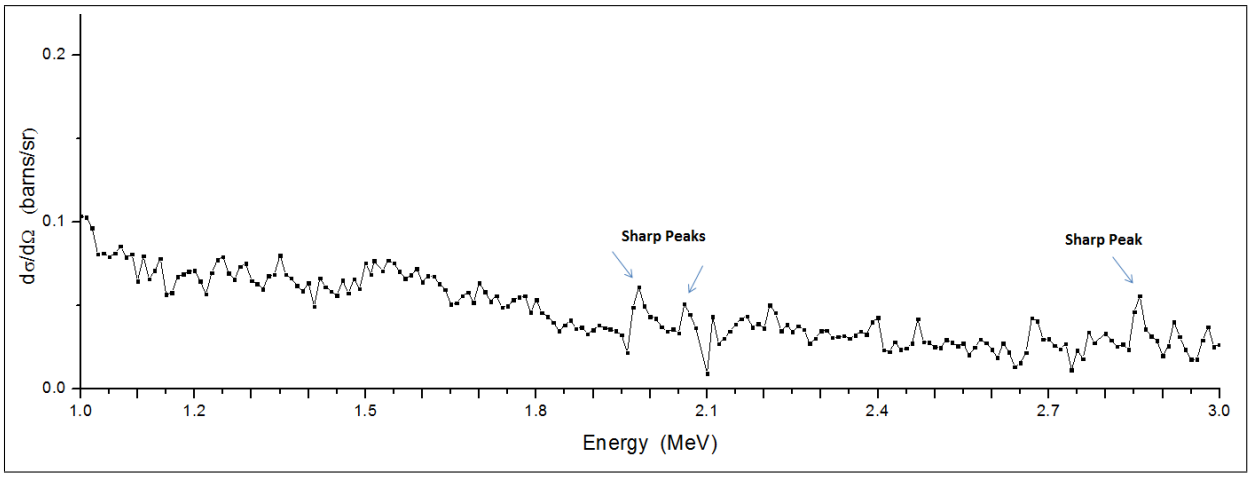

Fig. 5.1: Non-Rutherford Cross Section for Elastic Scattering of Protons from Aluminium at 140^0.

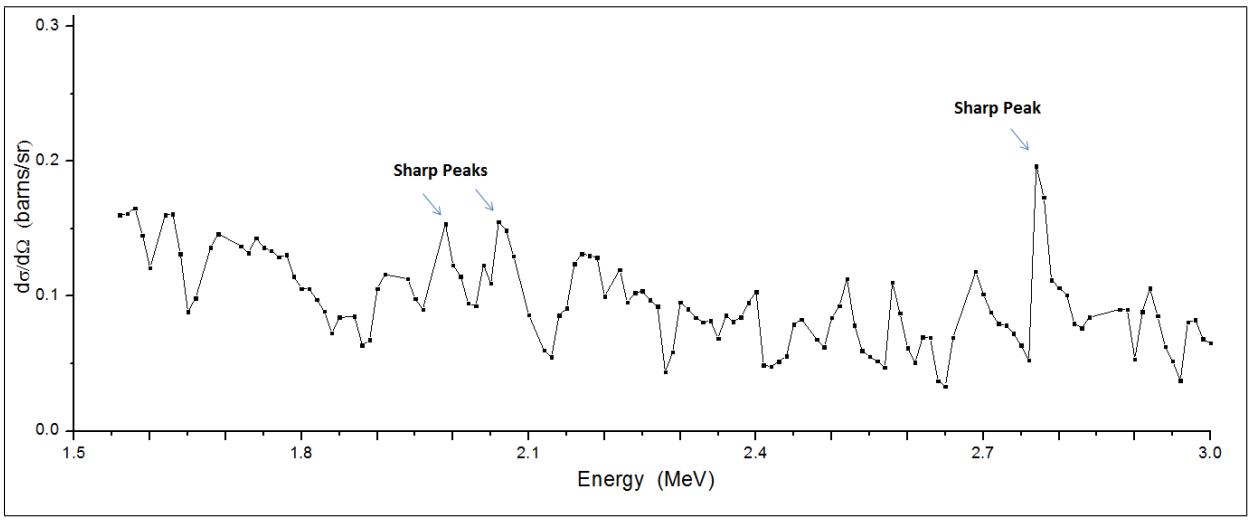

Fig. 5.2: Non-Rutherford Cross Section for Elastic Scattering of Protons from Aluminium at 170^0.

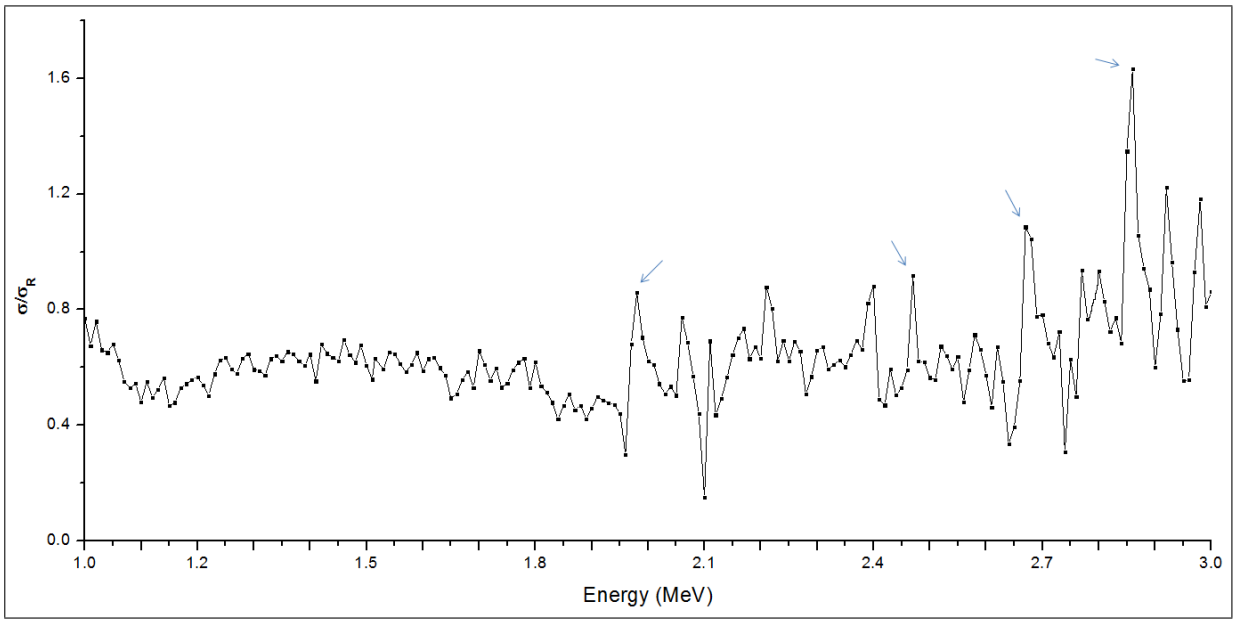

Fig. 5.3: Non-Rutherford to Rutherford Cross Sections Ratio for Elastic Scattering of Protons from Aluminium at 140^0. The arrows show the maximum deviation points.

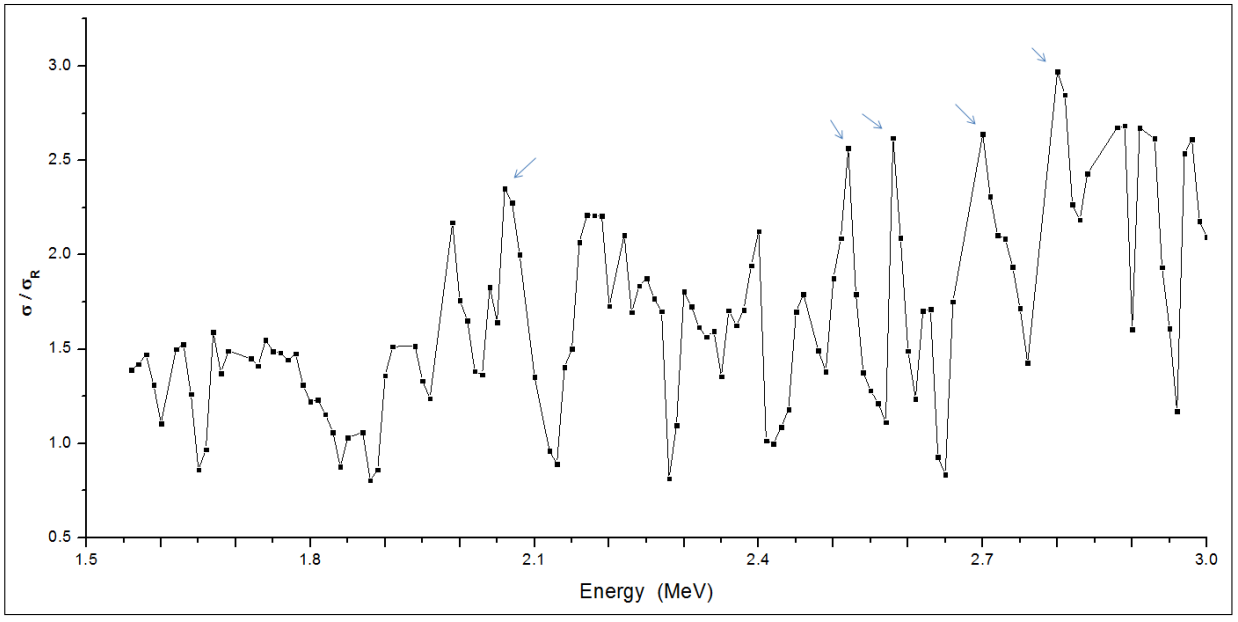

Fig. 5.4: Non-Rutherford to Rutherford Cross Sections Ratio for Elastic Scattering of Protons from Aluminium at 170^0. The arrows show the maximum deviation points.

The main results obtained in this experiment are:

- Graph of Non-Rutherford Cross Section 'σ' at 140^0 (fig. 5.1) shows sharp peaks near 2, 2.1 and 2.8 MeV. The values of Non-Rutherford cross sections in fig. 5.1 upto 1.9 MeV show fluctuations which may be due to some background noise. Some other sharp peaks are seen but of less amplitude or height then the above mentioned peaks. At 1 MeV, the cross section should approach Rutherford value of about 0.3 b/str, however the suppressed observed values by a factor of 3 show significant loss of scattered protons at this angle.

- Graph of Non-Rutherford Cross Section 'σ' at 170^0 (fig. 5.2) shows sharp peaks between 1.9 and 2.2 MeV and also near 2.8 MeV. There is more fluctuation in this graph which could possibly be due to inappropriate coating of aluminium layer on the target sample. Many sharp peaks are seen but they are of less magnitude then the above mentioned peaks. The overall magnitude of the Non-Rutherford cross sections in this graph is higher as compared to the previous graph.

- In the graph of Cross sections ratio '$\frac{\sigma}{\sigma_R}$' at 140^0 (fig. 5.3) the maximum deviation of data from Rutherford cross section is observed near 2.8 MeV and some other high deviations are near $2.7, 2.5$ and 2 MeV each. The values of the ratios of Non-Rutherford to Rutherford cross sections are mostly below 1 which is due to small Non-Rutherford Cross Section values discussed before. These deviation points shows resonances and the largest resonance is near 2.8 MeV of about 1.6 magnitude.

- In the graph of Cross sections ratio '$\frac{\sigma}{\sigma_R}$' at 170^0 (fig. 5.4) maximum deviation is near 2.8 MeV and other high deviations are near 2.5 and 2 MeV each. Similar to the Non-Rutherford Cross Section graph at the same angle there are also many fluctuations in this graph due to the fluctuation of Non-Rutherford Cross Section values. Majority of the data points in the graph are above 1 and the largest resonance has the magnitude around 3.

5.2 Comparison with Previous Papers

The present results are compared with past papers of M. Chiari [6], E. Rauhala [5] and A. R. Ramos [7]. M. Chiari has calculated proton elastic cross sections at laboratory angles of 135^0 and 170^0 from aluminium, E. Rauhala has calculated the cross section of proton elastic scattering from aluminium at laboratory angle of 170^0 while A. R. Ramos has calculated the ratios of Non-Rutherford to Rutherford cross sections at laboratory angles of 140^0 and 178^0. The present data is compared with the graphs of above mentioned papers. The graphs of M. Chiari, E. Rauhala and A. R. Ramos are obtained through taking images of the graphs from their papers. Then some careful editing is done to merge these graphs with our present data graphs. The color of the past paper graphs have been changed to red in order to differentiate them from our present data graphs. The comparison graphs are compared in the following sequence:

- Non-Rutherford Cross sections compared with Chiari at 140^0.
- Non-Rutherford Cross sections compared with Chiari at 170^0.
- Non-Rutherford Cross sections compared with Rauhala at 170^0.
- Non-Rutherford to Rutherford Cross sections ratios compared with Ramos at 140^0.
- Non-Rutherford to Rutherford Cross sections ratios compared with Ramos at 170^0.

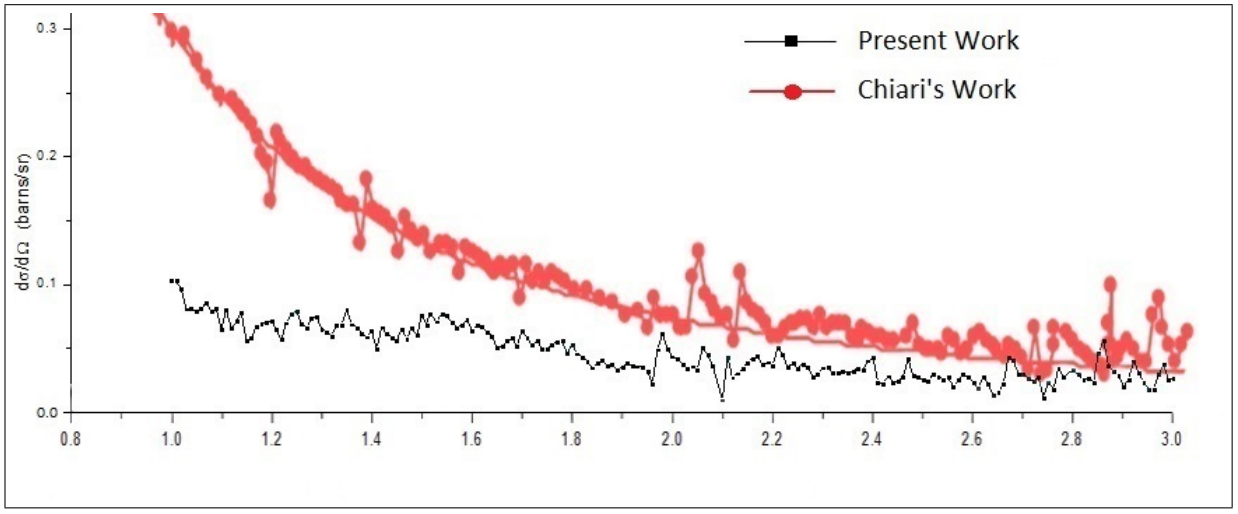

Fig. 5.5: Comparison of Non-Rutherford Cross Sections for Elastic Scattering of Protons from Aluminium at 140^0 with the cross section data of M. Chiari.

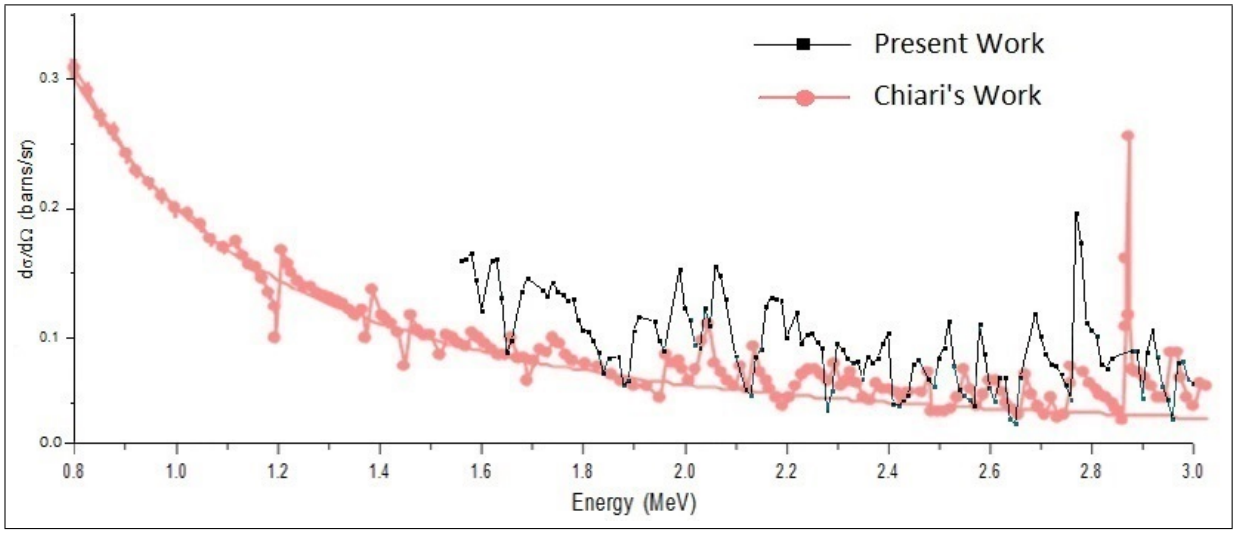

Fig. 5.6: Comparison of Non-Rutherford Cross Sections for Elastic Scattering of Protons from Aluminium at 170^0 with the cross section data of M. Chiari.

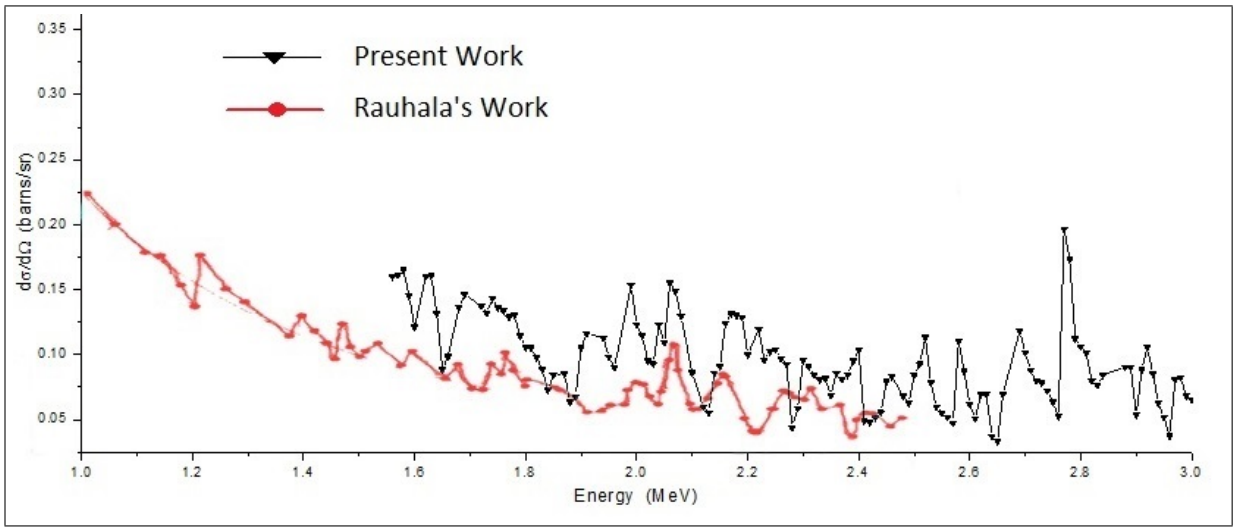

Fig. 5.7: Comparison of Non-Rutherford Cross Sections for Elastic Scattering of Protons from Aluminium at 170^0 with the cross section data of E. Rauhala.

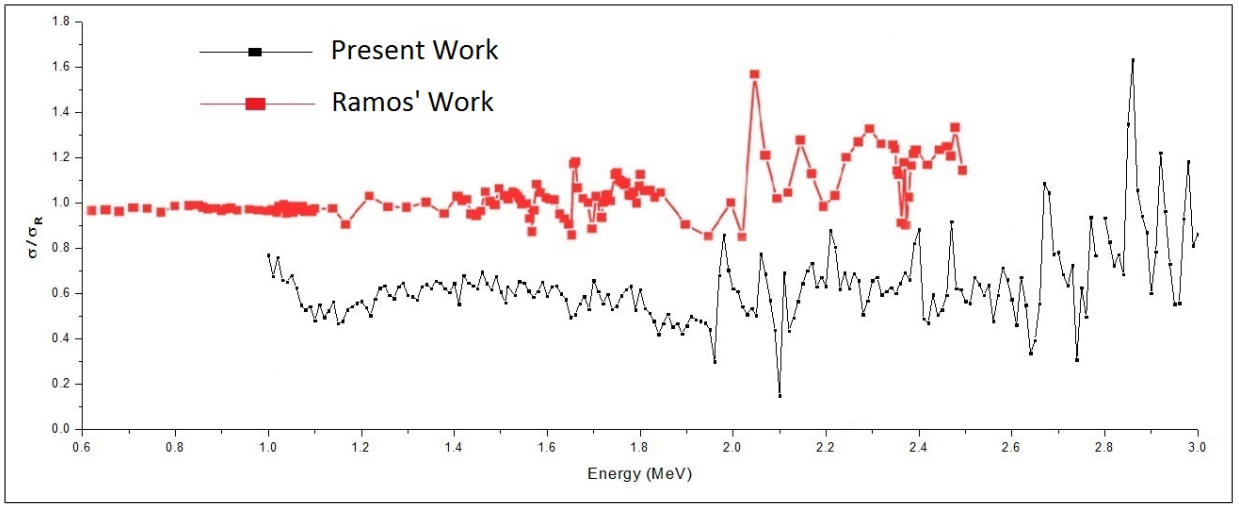

Fig. 5.8: Comparison of Non-Rutherford to Rutherford Cross Sections ratios for Elastic Scattering of Protons from Aluminium at 140^0 with A. R. Ramos.

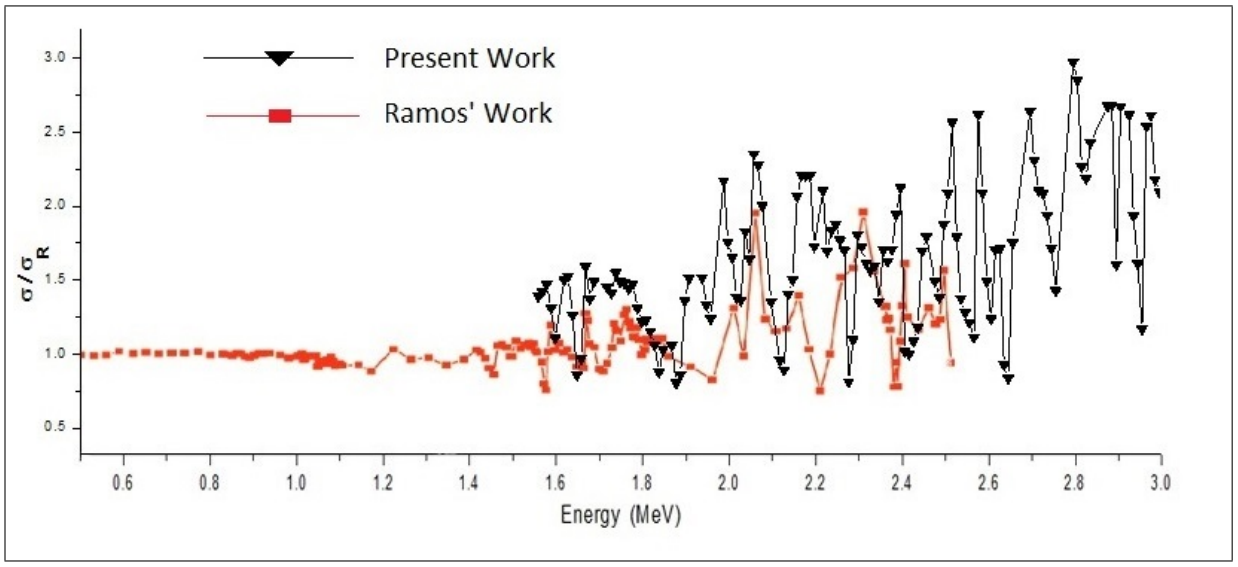

Fig. 5.9: Comparison of Non-Rutherford to Rutherford Cross Sections ratios for Elastic Scattering of Protons from Aluminium at 170^0 with A. R. Ramos.

From the above comparisons the following results are obtained:

- The comparison graph of Non-Rutherford Cross Section 'σ' with M. Chiari at 140^0 (fig. 5.5) shows decent that in the higher energies i.e. above 1.5 MeV the discrepancy between two experiments is considerably decreased. The sharp Non-Rutherford Cross Section peaks of present data and Chiari's data are seen at comparable energies. The difference between present data sharp peaks and M. Chiari's data sharp peaks of cross sections may be due to improper calibration of accelerator or detector or both. The magnitude of present data sharp peaks are relatively less then the magnitude of sharp peaks of M. Chiari's data due to possible loss of scattered flux at this angle. The majority or overall Non-Rutherford Cross Section values of present work are smaller then the overall Non-Rutherford Cross Section values of M. Chiari's data at 140^0.

- The comparison graph of Non-Rutherford Cross Section 'σ' at 170^0 with M. Chairi (fig. 5.6) shows better consistency as compared to Non-Rutherford Cross Sections comparison at 140^0. Again the difference between present data sharp peaks and M. Chiari's sharp peaks is seen whose possible reason is discussed before. The relative magnitude of sharp peaks of Non-Rutherford Cross Sections in present data is higher than the magnitude of sharp peaks of Non-Rutherford Cross Sections of M. Chiari's data except near 2.8 MeV, where present data sharp peak's magnitude is less then magnitude of the sharp peak of M. Chiari. The sharp peaks near 2.8 MeV are the largest ones in both graphs. The majority of the present data cross section values are larger then the cross section values of M. Chiari's data.

- The present work graph of Non-Rutherford Cross section 'σ' at 170^0 is also compared with E. Rauhala's graph whose data is upto 2.5 MeV. The graph (fig. 5.7) shows some consistency regarding the only Non-Rutherford Cross Section sharp peak near 2.1 MeV but the magnitude of present data sharp peak near 2.1 MeV is larger then the magnitude of the sharp peak of E. Rauhala's data. The majority of the values of present data Non-Rutherford

Cross Sections are larger then the Non-Rutherford Cross Section values of E. Rauhala's data.

- The comparison graph of Non-Rutherford to Rutherford Cross sections ratios '$\frac{\sigma}{\sigma_R}$' at 140^0 (fig. 5.8) does not show good agreement. There is no overlapping of the data points of the present graph with A. R. Ramos. The value of all present data points is smaller than Ramos' data whose possible reason is discussed before. The resonance peaks near 2 and 2.5 MeV are seen in both present data and Ramos' data. Despite the difference in the relative magnitudes of these resonance peaks, there is also difference in energies of the resonance peaks of Ramos' data and relative resonance peaks of present data. The possible reason is discussed before.

- The comparison graph of Non-Rutherford to Rutherford Cross sections ratios '$\frac{\sigma}{\sigma_R}$' at 170^0 of present data with A. R. Ramos' data (fig. 5.9) shows good agreement. The resonance peaks near 2.1 MeV and 2.5 MeV are seen on both data graphs. However the magnitudes of resonance peaks of present data are larger then the resonance peaks of Ramos. The overall data points are larger than Ramos' data points which is due to the fluctuation in Non-Rutherford Cross section at 170^0, the reason being discussed before.

- The overall results can be improved by reducing different kinds of errors. The proper calibration of accelerator's energy and detector's efficiency should be done. Careful handling of the samples during preparation and during experiment should be assured. Fresh samples should be used to reduce oxidation and other impurities mixing effect. The background noise was effecting the results so proper shielding of the detector should be ensured to reduce this effect. The detector's efficiency can be increased by decreasing the amount of current flowing towards it in a single step. The larger current makes the detector less efficient due to detector's dead time. Also small increments should be given in the input energy range for each step in order to have good results.

5.3 Conclusion

In spite of the limitations and constraints of the experimental setup, it is clear from the results that resonance scattering of protons can be observed and excited states of the target nucleus identified. This observation is critical for light element identification in complex targets, through back scattering experiments. The absolute values of cross sections and corresponding energy bins can be further improved with thorough analysis of the sources of experimental errors, which was beyond the scope of the present work. The results obtained and conclusions drawn can be summarized as follows:

- Non-Rutherford differential cross-sections were measured for Al (p,p) elastic scattering reaction at $E_P = 1$ MeV to 3 MeV in steps of 10 KeV at laboratory angles of 140^0 and 170^0.
- The ^{27}Al (p,p) ^{27}Al cross section has a lot of narrow resonances in the energy ranges of 1.9 MeV to 3.0 MeV.
- Overlapping of three resonances between energy range of 1.5 MeV and 1.8 MeV were observed due to effect of target thickness.
- It is well known that the Non-Rutherford and Rutherford Cross-Sections are inversely proportional to the square of projectile energy. The cross sections decrease with the increase in energy except at resonance points at which an abrupt increase in the Non-Rutherford Cross Section is observed due to the destructive interference between the coulomb and resonance scattering amplitudes. The elastic scattering yield as inverse of the square of incident energy could not be established within the energy range used.
- Differences in the Non-Rutherford Cross-Section values from theoretical Rutherford Cross-Section for energies near the resonant energy were observed for both scattering angles of 140^0 and 170^0.

- The resonance peaks confirm the effect of combined nuclear and coulomb forces in backscattering processes. Increase in amplitude of resonance peaks was observed at higher scattering angles.

- The comparisons of Non-Rutherford Cross Sections and Non-Rutherford to Rutherford Cross Sections ratios of present work with the work of M. Chiari, A. R. Ramos and E. Rauhala were made. The results showed a qualitative agreement with the existing data.

Bibliography

[1] T. R. Wilkins, *Phys. Rev.* **60**, (1941) 365.

[2] R. S. Bender, F. C. Shoemaker, S. G. Kaufmann and G. M. B. Bouricius, *Phys. Rev.* **76** (1949) 273.

[3] F . C. Shoemaker, J . E. Faulkner, G. M. B. Bouricius, S. G. Kaufmann and F. P. Mooring, *Phys. Rev.* **83** (1951) 1011.

[4] G. W. Greenlees, L. Giolietta Kuo and M. Petravic (Communicated by P. B. Moon, F. R. S. 1957).

[5] E. Rauhala, *Nucl. Instr. and Meth. B.* **40/41**, (1989) 790.

[6] M. Chiari, L. Giuntini, P. A. Mando, and N. Taccetti, *Nucl. Instr. and Meth. B.* **174**, (2001) 259.

[7] A. R. Ramos, A. Paul, L. Rijniers, M. F. da Silva and J. C. Soares, *Nucl. Instr. and Meth. B* **190** (2002) 95.

[8] Zdravko Siketic, Iva Bogdanovic Radovic, Natko Skukan, Milko Jaksic, and Ana Rita Lopes Ramos, *Nucl. Instr. and Meth. B* **261** (2007) 414.

[9] Kenneth S. Krane, *Introductory Nuclear Physics*, John Wiley and Sons, 1998.

[10] E. J. Burge, *Atomic Nuclei and Their Particles* , Oxford Science Publications, 2002.

[11] DOE Fundamentals Handbook, *Nuclear Physics And Reactor Theory Volume 1 of 2*, U.S. Department of Energy Washington, D.C. 20585, 1993.

[12] R. R. Roy and B. P. Nigam, *Nuclear Physics Theory And Experiment*, New Age International (P) Limited, Publishers, 1997.

[13] A. Das and T. Ferbel, *Introdution to Nuclear and Particle Physics* World Scientific Publishing Co. Pte. Ltd. 2005.

[14] P. E. Hodgson, *The Optical Model of Elastic Scattering*, Oxford, 1963.

[15] H. R. Verma, *Atomic and Nuclear Analytical Methods* Springer, 2007.

[16] R. Hellborg (Ed.), *Electrostatic Accelerators Fundamentals and Applications*, Springer, 2005.

[17] www.pelletron.com, *National Electrostatics Corporation (NEC)*, Last revised August 14, 2006 by *Tim Davis*.

[18] M. Bozoian, *Nucl. Instr. and Meth. B* **56/57** (1991) 740.